Open access • Journal Article • DOI:10.1061/(ASCE)GT.1943-5606.0001100

Experimental Investigation of Installation and Pullout of Dynamically Penetrating Anchors in Clay and Silt — Source link

Muhammad Shazzad Hossain, Youngho Kim, Christophe Gaudin

Published on: 01 Jul 2014 - Journal of Geotechnical and Geoenvironmental Engineering (American Society of Civil Engineers)

Topics: Embedment, Silt and Shear strength (soil)

Experimental Investigation of Installation and Pullout of Dynamically Penetrating Anchors in Clay and Silt

Muhammad Shazzad Hossain[1], Youngho Kim[2] and Christophe Gaudin[3]

Abstract: This paper reports the results from a series of model tests undertaken to provide insight into the behaviour of torpedo anchors during dynamic installation and pullout in lightly overconsolidated kaolin clay and calcareous silt. The tests were carried out in a drum centrifuge at 200 g, varying the drop height, hence the impact velocity, and the time delay for consolidation prior to pullout. The pullout angle at the mudline was also varied to encompass various mooring systems, including catenary (0°), taut leg (45°) and tension leg (~80°). Two geometries of torpedo anchors were explored, varying fin and tip geometry.

The results demonstrated that the anchor embedment depth increased as the drop height (and hence the impact velocity) increased and the soil undrained shear strength decreased. In stronger silt, the cavity above the installing anchor remained open whereas in soft clay, it was fully backfilled and replenished. The corresponding anchor embedment depth was also about 0.63 times compared to that in clay. The anchor holding capacity was found to increase with increasing post-installation consolidation time, depth of embedment and soil undrained shear strength and with reducing pullout angle at the mudline. The anchor rotation during pullout and hence the pullout distance for attaining the maximum capacity reduced as the load

[1] Corresponding Author, Associate Professor (BEng, MEng, PhD, MIEAust), ARC Postdoctoral Fellow, Centre for Offshore Foundation Systems (COFS), The University of Western Australia, 35 Stirling Highway, Crawley, WA 6009, Tel: +61 8 6488 7358, Fax: +61 8 6488 1044, Email: muhammad.hossain@uwa.edu.au

[2] Research Associate (PhD), Centre for Offshore Foundation Systems, The University of Western Australia, Email: youngho.kim@uwa.edu.au

[3] Professorial Fellow (PhD), Centre for Offshore Foundation Systems (COFS), The University of Western Australia, Email: christophe.gaudin@uwa.edu.au

inclination at the mudline increased. The fin geometry (rectangular or elliptical) and tip geometry (conical or ellipsoid) were shown to have remarkable influence on the holding capacity, with rectangular fins and conical tip proved to be more effective. The negligible adherence of silt along the anchor sides and the presence of semiliquid material around the extracting anchor resulted in a significantly (34~47%) lower holding capacity in the calcareous silt with significantly higher intact undrained shear strength.

CE Database subject headings: Anchors; Calcareous silts; Capacity; Centrifuge models; Clays; Impact velocity; Installation; Mooring; Offshore platforms; Pullout.

Introduction

Dynamically penetrating anchors (DPAs), colloquially referred to as torpedo anchors (see Figure 1), have been increasingly considered for deep water oil and gas development. The rapidly growing hydrocarbon exploration and extraction activity in deep and ultradeep water (now approaching 3000 m) and in emerging provinces has necessitated the development of alternative anchoring concepts. Among others, DPAs are the newest (late 90's; Lieng et al. 1999, 2000; Medeiros 2001, 2002) and are identified as the most promising concept due to (a) an economic, simple and quicker installation process performed by means of single anchor handling vessel (AHV) with no external energy source or mechanical operations required, (b) (and hence) a lower sensitivity to increasing water depth, (c) a high capacity under vertical and horizontal loading with no severe constraints about accurate positioning of the anchors on the sea bottom, (d) a flexibility in geometry that can accommodate a wide range of seabed strength (Medeiros 2002; Colliat 2002; Ehlers et al. 2004), and (e) a relatively lighter weight and inexpensive fabrication. Medeiros (2001) reported a related cost savings of 30% compared with conventional anchoring systems.

Anchor Installation

Typically a set of 4 to 8 anchors are transported to the location and deployed using a typical anchor handling vessel (see Figure 2). The dropping anchor is connected to an installation line and an independent mooring line. It is lowered to the pre-determined drop height above the seabed and then released by disconnecting the installation line. This allows the anchor to fall freely through the water column before impacting and embedding within the seafloor sediments. Penetration in the seabed is generated by the kinetic energy obtained through the free-fall and the self-weight of the anchor.

The main parameters that govern the penetration of a torpedo anchor in the seabed sediment include (a) the anchor mass, (b) the drop height and hence impact velocity at the mudline, (c) the anchor geometry, and (d) the soil strength and sensitivity, with the former was demonstrated to have the greatest influence (O'Loughlin et al. 2004; Richardson et al. 2006, 2009). Typical impact velocities vary between 10 and 30 m/s (Colliat 2002; Randolph et al. 2011) for free falling height ranging from 30 to 150 m. Anchor penetration in normally consolidated (NC) clay $d_{e,p}$ (to the top of the anchor) ranges from 8 m to 22 m. This results in a tip embedment $d_{e,t}$ up to 40 m or 2 to 3 times the anchor length (Colliat 2002). Dry weight of anchors ranges from 23 to 115 tonnes and anchoring capacities in NC clay lie between 3 and 5 times the dry weight.

Anchor Geometry

A typical DPA consists of a central shaft typically 0.75~1.2 m in diameter and 12~17 m long, and may feature stabilising fins. The cylindrical shaft is filled with scarp chain or concrete and covered by a lid attached with an omni-directional chain attachment point (i.e. padeye). In order to be applicable mostly in clayey sediments in increasing water depths, three alternative forms of DPAs have been proposed. They include (a) a pipe pile with a conical tip (angle 30~60°- TA1) (Medeiros 2002; de Araujo et al. 2004; Brandão et al. 2006), (b) a tube with a conical tip (angle 30~60°) and 4 rectangular fins attached at the upper part (TA2) (Medeiros 2002; de Araujo et al. 2004; Brandão et al. 2006), and (c) a tube with an ellipsoidal tip and 4 butterfly (TA3) or trapezoidal (TA4) wings attached at the trailing edge (Lieng et al. 1999, 2000, 2010). The rectangular (or trapezoidal) fins are 4 to 11 m in length and 0.45 to 0.9 m in width. They are now being tested to be considered in silty deposits (Medeiros 2002; Ehler et al. 2004). In this study, tests were carried out on model DPAs with 4 fins (TA2 and TA3).

74 ## *Applications*

75 To date, DPAs have been used for anchoring (i) flexible risers, ships, mono-buoys; (ii)
76 drilling MODUs and (iii) production FPUs. For the former instance, about 90 anchors were
77 installed from 2000 to 2001 (Medeiros 2002) and for the latter two, more than 50 torpedos
78 were installed from 2002 to 2005 (Brandão et al. 2006) in the Campos Basin, offshore Brazil.
79 Although mostly used in soft clay, torpedo anchors have been used to moor mono-buoys and
80 ships in shallow and deeper water in calcareous soils (Ehlers et al. 2004). As they are being
81 proven as an attractive and cost-effective alternative to more traditional anchoring solutions,
82 with the progress of maturity, torpedo anchors will be applicable for other floating facilities,
83 e.g. FPSOs, TLPs, SPAR platforms, and to various emerging new concepts, including floating
84 LNG (FLNG) facilities.

85 However, DPAs trail in the level of maturity and require the most technological development
86 to attain a mature state of practice similar to suction caissons. In an attempt to improve
87 maturity in design, future research activities for torpedo anchors are recommended to be
88 focused to: (a) improve understanding the performance during installation and under
89 operational loadings in calcareous and sandy soils, (b) improve the reliability in predicting
90 embedment depth and holding capacity, (c) determine the optimum number, size and
91 configuration of fins, and (d) develop corresponding design guidelines for the offshore
92 industry.

93

Review of Existing Data

Data from Field Test

Results from full scale field tests were reported by Medeiros (2002), de Araujo et al. (2004), Brandão et al. (2006) and Lieng et al. (2010). The aim was to evaluate the driveability and holding capacity of torpedo anchors (TA1, TA2, TA4). Tests were performed at the Campos Basin, offshore Brazil and at the Gjøa field in the North Sea, off the Western coast of Norway in water depths ranging from 200 m to 1200 m.

Installation: In order to assess the driveability, installation tests were carried out in various soils including (a) normally consolidated and overconsolidated clay (Marlim field), (b) 13 m thick fine sand layer overlying normally consolidated clay (Albacora field), and (c) uncemented calcareous sand (Corvina field) (Medeiros 2002). A finless pile of outer diameter (OD) D_A = 0.762 m and length L_A = 12 m (W_{dry} = 400 kN) was released from a drop height h_d = 30 m. The results illustrated in Figure 3a indicate that tip embedment of $d_{e,t} = 1.25L_A$ and $1.83L_A$ can be achieved in calcareous sand and sand-over-clay sediments, respectively.

For mooring Petrobras FPSO P-50, eighteen T-98 torpedo anchors (TA2, W_{dry} = 98 tonnes = 961 kN, D_A = 1.07 m, L_A = 17 m, four 0.9 m × 10 m rectangular fins) were installed successfully in soft normally consolidated clay ($s_u \approx 5 + 2z$ kPa) at the same basin (Albacora Leste field). They were released from a drop height of ~135 m. The achieved impact velocity was ~26.8 m/s, and the depths of final tip embedment were $d_{e,t}$ = 30~37 m (see Figure 3b). Trial tests were also performed varying the drop height (h_d = 40, 97, 135 m). The corresponding results are shown in Figure 3b. Broadly they show a trend - the impact velocity and anchor embedment depth increase with increasing drop height. However, the rate of increasing for the former is much higher compared to that for the latter.

In August 2009, two full scale 80 ton torpedo anchors (TA4, W_{dry} = 80 tonnes = 785 kN, D_A = 1.2 m, L_A = 13 m, four 1.4 m × 4~6 m trapezoidal fins) were successfully installed at the Gjøa field in the North Sea, off the Western coast of Norway, to tether an MODU (Lieng et al. 2010). Drop height of 50 and 70 m resulted in impact velocity of 24.5 m/s and 27 m/s and anchor tip embedment of 24 and 31 m, respectively. The undrained shear strength profiles more or less increased with depth as $s_u \approx 10 + 3.25z$ kPa and $s_u \approx 10 + 2.37z$ kPa, respectively. These are also included in Figure 3b for comparison. Although the trend is similar (and the data are limited), it is seen that much higher impact velocity was achieved at the Gjøa field for a similar drop height or in another words much lower drop height was necessary for achieving any impact velocity. The corresponding embedment depths at the Gjøa field were 12~30% lower, which may be due to the stronger seabed.

Theoretical prediction: As the anchor travels through water, its velocity increases and for a given drop height, h_d, the velocity at impacting the seafloor, v_i, can be calculated from hydrodynamic drag theory as

$$m\frac{d^2h_d}{dt^2} = W_s - \frac{1}{2}C_d\rho_w A_p v_i^2 \quad (1)$$

where m is the mass of the anchor, t is the time after releasing the anchor, W_s is the submerged weight of the anchor (in centrifuge tests the anchor dropped initially in air and then in water before impacting the soil surface and hence W_{dry} and/or W_s are used as appropriate), C_d is a dimensionless drag coefficient, A_p is the projected area of the anchor including the shaft and fins and ρ_w is the density of water. Note, for relatively higher drop heights, the anchor velocity may attain the terminal velocity (i.e. may not increase further with depth) before impacting the seabed. The predicted profiles using drag coefficient C_d = 0.6~3.04 are shown in Figure 3c. A value of C_d = 0.6~0.66 can be obtained matching with the

140 measured data in the North Sea and a much bigger value of 1.46~3.04 for the data in the
141 Campos Basin.

142 **Pullout:** Load tests were carried out in soft normally consolidated clay ($s_u \approx 5 + 2z$ kPa) at
143 Barracuda, Marlim, and Esdarte field in the Campos basin (Medeiros 2002). The tests were
144 performed using finless anchors (TA1, W_{dry} = 240, 620 kN, D_A = 0.76, 1.07 m, L_A = 12 m),
145 varying pullout angle (θ_0 = 0, 45 and 90°) and set-up time (10, 18 days). The normalised
146 results are plotted in Figure 3d, reflecting (a) a set-up factor of 2.13~2.21 for θ_0 = 0°,
147 2.16~2.47 for θ_0 = 45° and 5.05~5.73 for θ_0 = 90°, (b) a reduction of the pullout capacity as
148 the pullout inclination at the mudline rises from 0°.

149 ***Data from Centrifuge Test***

150 The pullout capacity of DPAs has been investigated experimentally through centrifuge model
151 testing (O'Loughlin et al. 2004; Richardson et al. 2006, 2009). The holding capacity, for a
152 given depth, increased with the number of fins due to the higher contact area (O'Loughlin et
153 al. 2004; de Aguiar et al. 2009) and reduced as the pullout inclination rises from the
154 horizontal (de Aguiar et al. 2009). As is generally the case for suction caissons, once the load
155 inclination exceeded about 30° to the horizontal, the capacity was governed entirely by the
156 vertical capacity.

157 Centrifuge work by Richardson et al. (2009) focused on the soil strength recovery after
158 installation and the subsequent holding capacity. As the anchor penetrated at high velocity,
159 significant soil disturbance was generated around the anchor and consolidation led to an
160 increase of anchor capacity with time, analogous to pile set-up. Results demonstrated a
161 significant increase of capacity with time (by a factor of 5 from immediate extraction to full
162 consolidation) but a greater period (up to 7 years for the 1.2 m diameter anchor presented here)

163 was required to achieve full consolidation compared with equivalent piles or suction caissons.
164 The reported outcomes will be discussed latter along with the results from this study.

165

166 ## Experimental Program

167 ### *Testing in Drum Centrifuge*

168 All tests were conducted at enhanced gravity in the drum centrifuge at the University of
169 Western Australia (Stewart et al. 1998). This allowed correct stress similitude; strength ratio,
170 $s_u/\gamma' D_A$, where s_u is the undrained shear strength and γ' the effective unit weight of the soil;
171 anchor mass; and drop height and hence impact velocity to be maintained between the model
172 experiments and offshore prototype conditions. Both the installation and the pullout tests were
173 carried out at a gravitational acceleration of 200 g, i.e. all prototype sizes are scaled down by
174 200, loads by 200^2 and mass by 200^3. Unless stated, all results are presented in prototype
175 dimensions. A ~15 mm (model scale) layer of water was maintained above the soil surface
176 during testing.

177 A total of 20 tests were carried out, including 11 tests on kaolin clay and 9 tests on calcareous
178 silt. Table 1 provides a summary of all tests conducted. Installation and subsequent pullout
179 were carried out on two anchor models, varying the drop height (h_d = 26~58 m without
180 applying spring tension and 61 m with applying spring tension; discussed later) and hence the
181 impact velocity (v_i = 14.94~22 m/s) and embedment depth ($d_{e,t}$ = 17.6~31 m), the elapsed
182 time before pulling out (t_c = 0.04~219.2 years), and the pullout angle at the mudline (θ_0 = 0,
183 45, 80°).

184 ### *Model Anchors*

185 Tests were undertaken using 1:200 scale model anchors of two different geometries (see
186 Figure 4). These include (a) a solid shaft with a conical tip (angle 30°) and 4 rectangular
187 vertical fins (W_{dry} = 1503 kN, D_A = 1.2 m, L_A = 15 m, L_F = 10 m, w_F = 0.9 m, t_F = 0.1 m –
188 referred to as model B) and (b) a solid shaft with an ellipsoidal tip and 4 butterfly vertical fins
189 (W_{dry} = 1726 kN, D_A = 1.2 m, L_A = 16.3 m, L_F = 7.4 m, w_F = 2.15 m, t_F = 0.1 m – referred to
190 as model N). The models were made from brass (density = 8400 kg/m^3). Table 2 summarises
191 the anchors geometry in model and prototype scale. The shapes were chosen similar to the
192 anchors in the field, TA2 and TA3, as illustrated by Medeiros (2002), de Araujo et al. (2004),
193 Brandão et al. (2006) and Lieng et al. (1999, 2000).

194 The anchor chain was modelled using braided fishing line, due to its flexibility, high tensile
195 strength, and resistance to stretching and unravelling.

196 ### *Release and Pullout Mechanism*

197 **Release system:** The Coriolis forces resulting from the rotating acceleration field in the
198 centrifuge requires the anchors to be installed through a guide to prevent lateral movement
199 during free fall. An installation guide was therefore manufactured from low friction PVC with
200 1 cylindrical groove with 4 wing channels in order to accommodate the 4-fin models, as
201 shown in Figure 5. The guide was 380 mm long and instrumented with a release system at the
202 back and a velocity measurement devises at the front. The release system consists of a spring,
203 a resistor (30 Ω) and a tightening screw. The anchor model's top (padeye) was attached with
204 two lines, including release line and pullout line similar to the field. The model was set in the
205 guide channels at a targeted drop height from the soil surface. The release string was carried
206 through a hollow piston attached with the spring, over the resistor, and finally knotted with

the screw (see Figure 5). The pullout string was left free. In some tests, the model was tensed against the spring by rotating the screw to increase the impact velocity and hence penetration depth.

As discussed previously, dynamic anchors rely upon the mass of the anchor and the velocity at impact with the seabed to achieve the required embedment. In the centrifuge, equivalent prototype impact velocities were obtained by allowing the anchor to free fall through the increased acceleration field from much lower drop heights. To measure the anchor velocity, while falling through the guide, 8 photoemitter-receiver pairs (PERPs, see Figure 5) were mounted at 12.5 mm intervals along the guide at its front edge, with the last pair being at 10 mm from the exit point. The time delay between the tip of the anchor model crossing the beam of two consecutive emitters enables the average velocity over that interval to be determined. In this way, the average velocity at multiple points down the guide can be determined, providing a velocity profile with vertical distance above the soil surface. The edge of the guide was set at a distance of 15 mm above the soil surface. The impact velocity was therefore calculated extrapolating this velocity profile.

A custom lock nut attached with a purpose-designed slotted plate was used to mount the whole installation system on the drum centrifuge tool table actuator.

Pullout system: For carrying out pullout tests at various angles, a frictionless pulley attached with a small slotted angle plate (allowed to adjust the position) was bolted at the edge either above or below (for 45~80° pullout and 0° degree pullout to the horizontal, respectively) the tool platform. The pullout string was carried over this pulley to the actuator, as illustrated in Figure 6. A 500 N load cell was incorporated in between the actuator and the pullout line (see Figure 6). This small load cell provided high resolution of the measured load response.

Testing Procedure

The anchor was put inside the guide at a given drop height. It was held in position by using the release string attached to the screw (see Figure 5). The installation guide was positioned at the test site. The anchor release in flight was triggered by the resistor, which then supplied with current, heated up and subsequently burnt through the release string. This allowed the anchor model to free fall, initially through the guide and then through the water column, before impacting the soil and coming to rest at a depth within the sample.

The centrifuge was ramped down so the crater above the installed anchor could be monitored. The pullout string was stretched manually to (a) measure the depth of embedment and (b) remove any slack. The tool platform was move up or down to set the pullout angle at the mudline. The string was then linked to the load cell over the pulley (see Figures 6 and 7). This allowed for maintaining the inclination constant during pulling out the anchor. The centrifuge was then ramped up again back to 200 g. A period was then allowed for dissipation of the excess pore water pressures (up to a certain degree) induced by the installation process around the anchor. At completion of the reconsolidation period, the pullout test commenced. The corresponding load-displacement was recorded.

The undrained pullout capacity of the anchors was evaluated by vertical monotonic extraction at a rate of 2 mm/s. This rate was selected such that the normalised velocity index during extraction, $V = vD_A/c_v$ (where v is the extraction rate, D_A the anchor diameter and c_v the vertical coefficient of consolidation at the average anchor penetration; see Tables 2~4), = 31 and 144 > 30, which was expected to be sufficient to ensure undrained conditions both in clay and silt according to Finnie (1993).

252 ### *Preparation of Sample*

253 The tests were performed in lightly overconsolidated kaolin clay and calcareous silt, with the
254 engineering properties given in Tables 3 and 4, respectively. Both samples were prepared
255 together following an identical procedure. A homogeneous slurry was prepared by mixing
256 commercially available kaolin clay powder with water at 120% water content (twice the liquid
257 limit) and subsequently de-airing it under a vacuum. The silt material used was dredged
258 directly from the Australian seabed.

259 The channel was divided into two compartments by using two smooth aluminium plates to
260 deposit clay and silt (see Figure 8). The clay and silt slurries were then placed carefully into
261 the compartments alternatively, ensuring the balance of the channel. Normally consolidated
262 samples with a linearly increasing strength profile were produced by performing
263 consolidation at 200 g for seven days. The resulting clay and silt samples were 160 and
264 170 mm deep, respectively. The upper ~5 mm of the normally consolidated samples were
265 scraped off to achieve slight overconsolidation and a levelled surface for testing. For
266 calcareous silt, the carefully prepared soil sample may have produced engineering behaviour
267 corresponding to anchor installation and pullout consistent to the field seabed with similar
268 undrained shear strength.

269 ### *Soil Strength Determination*

270 Site characterisation tests were carried out in-flight using a T-bar penetrometer of diameter
271 5 mm and length 20 mm (model scale). These tests were conducted at a rate of 1 mm/s, which
272 was sufficiently fast to ensure undrained behaviour in both the kaolin and the silt. Figure 9
273 shows inferred strength profiles based on a T-bar factor of $N_{T\text{-}bar} = 10.5$. The strength values
274 may be idealised linearly increasing with depth as $s_u = 1 + 0.85z$ kPa (clay) and $2 + 3z$ kPa

(silt). The strength profiles replicated those typically found in offshore case studies (Randolph 2004).

Installation of Anchors

Impact Velocity

The anchor velocity at impact was determined from the velocity profile established from the PERPs (see Figure 10a). A theoretical velocity profile was established, accounting for the non-uniform acceleration field, which was fitted to the experimental velocity values and permitted, by extrapolation, to determine the anchor velocity at impact. In the centrifuge, the gravitational acceleration, a, increases with the radius, R, according to

$$a = \omega^2 R \tag{2}$$

where ω is the centrifuge angular velocity in rad/s. Consequently, the anchor experiences an increasing gravitational acceleration as it falls towards the soil. The anchor velocity during free fall was therefore calculated using the approach given below. The velocity, v_k, at the end of an increment was a function of the velocity, v_0, the average acceleration, a, over the increment (i.e. average of a_k:a_0), and the radius increment, ΔR, from the onset (i.e. R_k - R_0), as follows

$$v_k = \sqrt{v_0^{\,2} + 2a(R_k - R_0)} \tag{3}$$

Note that this does not account for the (negligible) deceleration experienced by the anchor as it penetrated from air to the thin water layer above the soil surface. The theoretical velocity profiles required adjustment to account for friction along the anchor-guide interface. An example profile plotted in Figure 10a demonstrates the full installation features for Test C7. Table 1 shows the range of impact velocities measured during the anchors installation and the

297 dependence of impact velocity (v_i) on the anchor drop height (h_d). The achieved impact
298 velocities vary between 15 and 22 m/s (see Table 1), and increase with drop height. In some
299 tests on silt, the anchor model was pulled against the spring prior to releasing, which led to
300 obtain a slightly higher impact velocity and hence embedment depth (see Table 1).

301 These values of impact velocity and prototype equivalent drop height (accounting for the non-
302 uniform acceleration field), along with theoretical prediction using Equation 1 and $C_d = 0.24$
303 (note, the radius to the soil surface limits the curve length), are plotted in Figure 10b. The
304 discrepancy between the measured data and theory is about 10~15%, which can be attributed
305 to the friction that developed along the anchor-guide interface, as also commented on by
306 O'Loughlin et al. (2004). A comparison between the values from this study and the reported
307 data from model tests by Richardson (2008) and field tests by de Araujo et al. (2004),
308 Brandão et al. (2006) and Lieng et al. (2010) are shown in Figure 10c. They all show a
309 consistent trend except the data reported by Brandão et al. Apparently, the velocities 24~27
310 m/s attained the terminal one as they did not increase further with drop height.

311 ***Embedment Depth***

312 The corresponding embedment depths are plotted in Figure 11. The anchor penetration depth
313 increases as the impact velocity (and hence drop height) increases. For silt ($s_u = 2 + 3z$ kPa),
314 the anchor tip embedment ($d_{e,t}$) is about 1.17~1.4L_A. For softer clay with $s_u = 1 + 0.85z$ kPa,
315 the depth is significantly higher and, for a similar velocity, it is around 1.6 times of that for
316 silt. However, under these impact velocities, in most case, the embedment depth (~2L_A) was
317 restricted by the clay sample depth of 31 m (~2L_A). Nevertheless, it is believed that the
318 consequent effect (if any) on the anchor pullout resistance was minimal and was not obvious
319 from the extraction profiles presented later.

The above results are for model B. For lower impact velocities and in stronger calcareous silt, slightly higher embedment depths were obtained for the heavier model N (see Tests K10, K11, C3, C9; Table 1).

Similar to Figure 10, centrifuge and field test data from the literature are incorporated in Figure 11 for comparison. The tip embedment depths for a relatively lighter anchor (15.5 gm compared to 19.16~22.01 gm) in clay with s_u = ~1.35z kPa (which lies between achieved strengths in this study of 1 + 0.85z kPa and 2 + 3z kPa), as reported by O'Loughlin et al., lie between the trend for clay and silt. Field data for an anchor (W_{dry} = 78 tonnes compared to 153~160 tonnes) in clay (s_u = 5 + 2z kPa) show a trend consistent to the measured data in clay.

Installation Mechanism: Cavity Condition

Model tests were carried out inside the body of the soil deposited around the drum channel (see Figure 8), which prevented photos of installation mechanism to be captured. However, the top view of the failure mechanisms were recorded continuously by using a camera mounted on the tool platform as well as capturing photos after the completion of each test. The centrifuge was stopped after each installation test for setting-up to carry out pullout test, as discussed previously. It was seen that, in silt, a cavity formed above the installed anchor remained open and, in clay, the top was fully covered or replenished (i.e. no cavity), as displayed in Figure 12. The open cavity remained stable during the whole consolidation time, as monitored by the camera. This is critical both for installation and pullout as

(a) During installation, the weight of the backfilled/infill soil (if any) above the installing anchor will augment the vertically downward load (weight of anchor) and hence the embedment depth. This may be partly responsible for the deeper embedment depths in clay, and is reflected in Figure 11.

(b) During pullout, for clay, the weight of the backfilled/infill soil will act against extraction. Some researchers (e.g. Richardson et al. 2009's Equation 4) suggest to take into account (either shallow or deep) bearing resistance at the padeye level. This relies on the presence of soil above the shaft and fins. Conversely, for silt the open cavity was filled with water and hence the bearing resistance at the top of the shaft and fins could not be mobilised. Furthermore, the backfilled/infill soil provides a seal over the top of the anchor shaft and fins, which ensures transient suctions (constituted by reverse end bearing) to be sustainable beneath the anchor. In absence of this sealing, the consequential contribution to the pullout capacity and (possibly) frictional resistance along the surfaces of the anchor were lower.

Pullout of Anchors

The extraction resistance from anchor pullout tests are presented in terms of normalised response, $F/(A_p s_{u,av})$ (where F is the extraction resistance and $s_{u,av}$ is the average undrained shear strength over the anchor shaft length i.e. at the mid height of the anchor shaft), as a function of normalised pullout displacement, u/D_A. The ultimate holding capacity including the form of pullout response of anchors is affected by a number of factors: (a) the type of the soil deposit; (b) the angle of pullout at the mudline, θ_0; (c) the time allowed for reconsolidation, t_c; and (d) the geometry of the model anchor. In the following sub-sections, the results will be discussed in relation to these various factors.

Effect of Soil Type

In order to highlight the effect of soil type the normalised pullout resistances from Tests K7, K9 (clay) and C5, C8 (silt) are plotted in Figure 13 ($\theta_0 = 45°$; Table 1). The form of response

366 profile for silt is more gradual and less brittle compared to that for clay. The displacements
367 required for achieving the holding capacity, for a given inclination, are consistent. In
368 calcareous silt, the anchor was shallowly embedded ($d_{e,t}/L_A$ = 1.17~1.4), and an open cavity
369 was existed above the installed anchor whereas, in clay, the anchor was deeply embedded
370 ($d_{e,t}/L_A$ = 1.89~2), and fully buried. As discussed previously, the lack of sealing above the
371 anchor, caused by the water filled cavity, has significant influence on the mobilised skin
372 friction along the surfaces and suction at the base of the anchor. Furthermore, a number of
373 researchers (e.g. Erbrich and Hefer 2002, Cassidy 2012) have noticed that the mobilised
374 friction in calcareous silt is much lower than that in clay. This is also demonstrated in Figure
375 7 by (a) no or negligible adhered soil along the sides of the extracting anchor, and (b) the
376 presence of semi-liquid soils around the extracting anchor. The net resultant is, for similar t_c,
377 the holding capacity in calcareous silt is only 0.5~0.7 times of that in clay.

378 ***Effect of Pullout Angle at the Mudline, θ_0***

379 Pullout tests were carried out at θ_0 = 0, 45 and 80° in an attempt to cover catenary, taut-leg
380 and tension leg moorings. The results for Tests K2, K4, K7 and C3, C4, C5 (model B, Table 1)
381 are shown in Figures 14a and 14b, respectively, to examine the effect of loading angle. The
382 form of extraction resistance changes with the loading inclination. In general, as the load
383 inclination reduces, the curve becomes more gradual, reflecting that an increasing degree of
384 rotation was required for the anchor to be aligned with the pulling line. Consequently, the
385 required displacement to attain the peak capacity (referred to as holding capacity) is greater
386 for lower pullout angle. The most brittle response corresponds to 80° inclination i.e. it rises
387 quickly to the peak value followed by a sharp drop. This is caused by somewhat no rotation
388 and (hence) less adherence of soil along the extracting anchor sides (see insert of Figures 6a
389 and 7a). The holding capacity, for a given embedment depth, reduces as the pullout

390 inclination rises from the horizontal. This is because the corresponding soil failure mechanism
391 changes (and becomes more confined) and degree of rotation and adherence reduce. Note, the
392 time allowed for consolidation (t_c) for each test is also different.

393 By comparing the responses, once again, the normalised holding capacities in calcareous silt
394 are ~50% of that in clay.

395 ***Effect of Time Allowed for Reconsolidation, t_c***

396 In order to illustrate the effect of the reconsolidation time, t_c on the extraction resistance, the
397 results of various reconsolidation times t_c = 0.04, 2.28, 9.13, 109.59 (θ_0 = 0°, models B and N,
398 clay and silt, Tests K3, K10 and C1, C4; Table 1) and 0.04, 82.2 (θ_0 = 45°, model B, clay and
399 silt, Tests K7~K9 and C5, C8; Table 1) are displayed in Figures 15a and 15b, respectively.
400 This noted time does not include the required for ramp down, anchor set-up and ramp up back
401 to 200 g, which was around 20 minutes. Installation of the anchor models induced excess pore
402 water pressures. The time before pulling out allowed for dissipation of that excess pore
403 pressures up to a certain degree and hence gain in soil strength, as also observed from T-bar
404 tests by Hodder et al. (2010). Consequently, the holding capacity should increase with time.
405 Indeed, for kaolin clay, similar normalised holding capacity can be obtained for identical t_c
406 (see Figure 15b) and that increases with increasing t_c (see Figures 15a and 15b). However, for
407 silt, the percentage of increase is much lower - around 1/3 of that for clay. It is believed that (a)
408 the high permeability and c_v of silt and (b) the open cavity above the anchor allowed for
409 accelerating the reconsolidation process.

410 The holding capacities are normalised as

411 $$F_N = \frac{F - W_s}{s_{u,av} A_p} \quad (4)$$

412 and plotted in Figure 16 against non-dimensional time, $T = c_h t_c/D_A^2$, where c_h is the horizontal
413 coefficient of consolidation, which can be approximately calculated from c_v by multiplying
414 with $\sqrt{5}$ (Schneider et al. 2008; Richardson et al. 2009). Richardson et al. (2009) reported
415 vertical pullout capacity from model tests in kaolin clay. They are also included in Figure 16
416 for comparison. The values from this study are much scattered as they are for various load
417 inclinations θ_0 = 0, 45, 80°. Richardson et al.'s capacity values lie below as they are from
418 vertical pullout tests (θ_0 = 90°).

419 The set-up factor is difficult to calculate as tests were carried out at various load inclinations
420 and no immediate pullout was conducted.

421 ***Effect of Model Anchor Geometry***

422 The tests were carried out using two model anchors – model B and N. The effect of anchor
423 geometry on the form of extraction resistance profile, including the holding capacity, are
424 shown in Figures 17a and 17b for pullout inclination of θ_0 = 0° and 45°, respectively (clay,
425 Tests K2, K3 and K6, K7; Table 1). The form of extraction profile and pullout displacement
426 for attaining the ultimate capacity are similar for both model anchors. The latter one is slightly
427 heavier and longer, resulting in greater embedment depth although the tip is elliptical
428 compared to conical for model B (see Table 1). Even then, for similar t_c, the normalised
429 holding capacity (including F_N) for model N is about 0.75~0.78 times of that for model B
430 regardless of pullout angle. As such, anchor model B may be more effective in the field.

431

Concluding Remarks

This paper has reported results from centrifuge model tests investigating dynamic installation and monotonic pullout of torpedo anchors in lightly over consolidated clay and calcareous silt. The tests were carried out varying the drop height, hence the impact velocity, and the time delay for reconsolidation prior to pullout. The pullout angle at the mudline was also varied to encompass various mooring systems, including catenary (0°), taut leg (45°) and tension leg (~80°). The following key conclusions can be drawn from the results presented in the paper.

The achieved impact velocities were 15~ 22 m/s, which increased with increasing drop height. These values were found to be consistent with the reported centrifuge model test data and field data. They were 10~15% lower than theoretical prediction (using C_d = 0.24) due to frictional loss in the launcher guide.

The anchor embedment depth increased with increasing drop height (and hence the impact velocity) and decreasing soil undrained shear strength. The anchor tip embedment ($d_{e,t}$) was about 1.17~1.4L_A in calcareous silt (with s_u = 2 + 3z kPa). In softer clay with s_u = 1 + 0.85z kPa, the embedment, for a similar impact velocity, was around 1.6 times compared to that in silt.

In stronger silt, the cavity above the installing anchor remained open whereas in soft clay, it was fully backfilled and replenished. This is critical both for installation and pullout. During installation, the backfilled/infill soil above the anchor augments the vertically downward load. During extraction, that soil provides a seal over the top of the anchor shaft and fins, which may lead reverse bearing to be mobilised at the base of the anchor shaft and fins and higher skin friction along the anchor surfaces.

The anchor holding capacity increased with increasing post-installation consolidation time, depth of embedment and soil undrained shear strength and with reducing pullout angle at the mudline. The fin geometry (rectangular or elliptical) and tip geometry (conical or ellipsoid) were shown to have remarkable influence on the holding capacity. The normalised holding capacity for anchor model N was about 0.75~0.78 times of that for model B, regardless of pullout angle, and hence model B may be more effective in the field.

The negligible adherence of silt along the anchor sides and the presence of semiliquid material around the extracting anchor resulted in a significantly (34~47%) lower holding capacity in the calcareous silt with significantly higher intact undrained shear strength.

To develop design approaches for anchor installation and pullout, an extensive investigation is being carried out through 3D large deformation FE analyses, validating against these centrifuge test data. The results will be published in a forth coming paper.

Acknowledgements

The research presented here was undertaken with support from the University of Western Australia through the ECM Research Development Grant (ECM RDG10300048). The first author is an ARC Postdoctoral Fellow (APDI) and is supported by the ARC Linkage Project LP110100174. The work forms part of the activities of the Centre for Offshore Foundation Systems (COFS), currently supported as a node of the Australian Research Council Centre of Excellence for Geotechnical Science and Engineering, through Centre of Excellence funding from the State Government of Western Australia and in partnership with The Lloyd's Register Foundation. This support is gratefully acknowledged, as is the assistance of the drum centrifuge technician, Mr. Bart Thompson.

Notation

a	gravitational acceleration
A_P	anchor projected area including shaft and fins
c_h	horizontal coefficient of consolidation
c_v	vertical coefficient of consolidation
C_d	dimensionless drag coefficient
d_e	embedment depth of installed anchor
$d_{e,t}$	embedment depth of installed anchor tip
$d_{e,p}$	embedment depth of installed anchor padeye
D_A	anchor shaft diameter
F	extraction resistance
F_N	normalised holding capacity
h_d	drop height
L_A	anchor shaft length
L_F	fin length
L_T	anchor shaft tip length
m	anchor mass
R	radius

495	s_u	undrained shear strength
496	$s_{u,av}$	average undrained shear strength over anchor shaft length
497	t	time after releasing the anchor
498	t_c	time allowed for reconsolidation before pulling out
499	t_F	fin thickness
500	T	non-dimensional time
501	u	pullout distance
502	v	extraction rate
503	v_i	anchor velocity at impact
504	v_0, a_0, R_0	velocity, acceleration and radius at the beginning of anchor drop
505	v_k, a_k, R_k	velocity, acceleration and radius at the end of each increment
506	V	non-dimensional velocity index
507	w_F	fin width
508	W_{dry}	anchor dry weight
509	W_s	anchor submerged weight
510	z	depth below soil surface
511	γ'	effective unit weight of soil
512	ρ_w	density of water

513 θ_0 pullout angle at mudline

514 ω centrifuge angular velocity

References

Brandão, F. E. N., Henriques, C. C. D., de Araujo, J. B., Ferreira, O. C. G. and dos Santos Amaral, C. (2006). "Albacora Leste Field Development – FPSO P-50 Mooring System Concept and Installation." *Proc. Offshore Technology Conference*, Houston, OTC 18243.

Cassidy, M. J. (2012). "Experimental observations of the penetration of spudcan footings in silt." *Géotechnique* 62(8), 727-732.

Colliat, J. L. (2002). "Anchors for Deepwater to Ultradeepwater Moorings." *Proc. 34th Offshore Technology Conference*, Houston, Paper No. 14306.

de Araujo, J. B., Machado, R. D. and de Medeiros Junior, C. J. (2004). "High Holding Power Torpedo Pile – Results for the First Long Term Application." *Proc. 23rd Int. Conf. Offshore Mechanics and Arctic Engineering*, OMAE, Vancouver, OMAE 2004-51201.

de Aguiar, C. S., de Sousa, J. R. M, Ellwanger, G. B., Porto, E.C., Junior, C. J. and Foppa, D. (2009). "Undrained load capacity of torpedo anchor in cohesive soils." *Proc. 28th Int. Conf. Offshore Mechanics and Arctic Engineering*, OMAE, Honolulu, OMAE 2009-79465.

Ehlers, C. J., Young, A. G. and Chen, J. H. (2004). "Technology Assessment of Deepwater Anchors." *Proc. 36th Offshore Technology Conference*, Houston, Paper No. 15265.

Erbrich, C. and Hefer, P. (2002). "Installation of the Laminaria suction piles – a case history." *Proc. Offshore Technology Conference*, Houston, Paper No. OTC 14240.

536 Finnie, I. M. S. (1993). "*Performance of Shallow Foundations in Calcareous Soil*." PhD
537 Thesis, The University of Western Australia.

538 Hodder, M. S., White, D. J. and Cassidy M. J. (2010). "Analysis of Soil Strength Degradation
539 during Episodes of Cyclic Loading, Illustrated by the T-bar Penetration Test." *Int. J.*
540 *Geomechanics* 10(3), 117-123.

541 Lieng, J. T., Tjelta, T. I. and Skaugset, K. (2010). "Installation of Two Prototype Deep
542 Penetrating Anchors at the Gjoa Field in the North Sea." *Proc. Offshore Technology*
543 *Conference*, Houston, Paper No. 20758.

544 Lieng, J. T., Kavli, A., Hove, F. and Tjelta, T. I. (2000). "Deep Penetrating Anchor: Further
545 Development, Optimization and Capacity Clarification." *Proc. 10th Int. Offshore and*
546 *Polar Engineering Conference*, Seattle, USA, pp. 410-416.

547 Lieng, J. T., Hove, F. and Tjelta, T. I. (1999). "Deep Penetration Anchor: Subseabed
548 Deepwater Anchor Concept for Floaters and other Installations." *Proc. 9th Int.*
549 *Offshore and Polar Engineering Conference*, Brest, France, pp. 613-619.

550 Medeiros Jr., C. J. (2002). "Low Cost Anchor System for Flexible Risers in Deep Waters."
551 *Proc. 34th Offshore Technology Conference*, Houston, Paper No. 14151.

552 Medeiros Jr., C. J. (2001). "Torpedo Anchor for Deep Water." *Proc. DOT Conference*, Rio de
553 Janeiro.

554 O'Loughlin, C. D., Randolph, M. F. and Richardson, M. D. (2004). "Experimental and
555 Theoretical Studies of Deep Penetrating Anchors." *Proc. 36th Offshore Technology*
556 *Conference*, Houston, USA, Paper No. 16841.

557 Randolph, M. F., Gaudin, C., Gourvenec, S. M., White, D. J., Boylan, N. and Cassidy M. J.
558 (2011). "Recent Advances in Offshore Geotechnics for Deep Water Oil and Gas
559 Developments." *Ocean Engineering* 38(7), 818-834.

560 Richardson, M. D. (2008). "*Dynamically Installed Anchors for Floating Offshore Structures*."
561 PhD Thesis, The University of Western Australia.

562 Richardson, M. D., O'Loughlin, C. D., Randolph, M. F. and Cunningham, T. J. (2006).
563 "Drum Centrifuge Modelling of Dynamically Penetrating Anchors." *Proc. Int. Conf.*
564 *Physical Modelling in Geotechnics*, Hong Kong, pp. 673-678.

565 Richardson, M. D., O'Loughlin, C. D., Randolph, M. F. and Gaudin, C. (2009). "Setup
566 following Installation of Dynamic Anchors in Normally Consolidated Clay." *Journal*
567 *of Geotechnical Geoenvironmental Engineering*, *ASCE* 135(4), 487-496.

568 Schneider, J. A., Randolph, M. F., Mayne, P. W. and Ramsey, N. R. (2008). "Analysis of
569 factors influencing soil classification using normalised piezocone tip resistance and
570 pore pressure parameters." *J. Geotechnical and Geoenvironmental Engineering, ASCE*
571 134(11), 1569-1586.

572 Stewart, D. P. (1992) "*Lateral Loading of Piled Bridge Abutments due to Embankment*
573 *Construction*." PhD Thesis, The University of Western Australia.

574 Stewart, D. P., Boyle, R. S. and Randolph, M. F. (1998). "Experience with a New Drum
575 Centrifuge." *Proc. Int. Conf. Centrifuge '98*, Rotterdam: Balkema. pp. 35-40.

576

577 **Table 1.** Summary of centrifuge tests conducted

Event	Test	Model anchor	Drop height, h_d		Impact velocity, v_i (m/s)	Depth of tip embedment, $d_{e,t}$		Time allowed for consolidation, t_c^+		Pullout angle, θ_0 (°)	Holding capacity, F/A_p (kPa)
			Model (mm)	Prototype* (m)	Model = Prototype	Model (mm)	Prototype (m)	Model (hrs)	Prototype (yrs)		
E1: Kaolin clay	K1	B	260	32.59	18.55	149	29.8	0.5	2.28	45	-
	K2	B	260	32.59	18.57	150	30	0.5	2.28	0	4276.69
	K3	N	255	32.22	18.75	151.5	30.3	0.5	2.28	0	3373.09
	K4	B	260	32.59	18.6	151	30.2	0.5	2.28	80	2991.71
	K5	N	260	32.59	18.9	155	31	0.5	2.28	80	2291.52
	K6	N	260	32.59	18.8	154	30.8	48	219.18	45	2901.60
	K7	B	255	32.22	18.36	150	30	18	82.19	45	3557.59
	K8	B	175	24.99	15.7	145	29	0.0083	0.038	45	2847.59
	K9	B	133.32	20.18	14.94	142	28.4	0.0083	0.038	45	2758.08
	K10	N	175	24.99	15.85	151.5	30.3	24	109.59	0	4095.64
	K11	B	180	25.52	15.83	145	29	24	109.59	0	-
E2: Calcareous silt	C1	B	273	32.82	19.08	100	20	0.0083	0.038	0	3970.99
	C2	N	305	34.55#	22	117	23.4	18	82.19	80	2655.07
	C3	B	305	34.63#	21.22	106	21.2	0.0083	0.038	80	3034.95
	C4	B	305	34.63#	21.15	104.5	20.9	2	9.13	0	4423.09
	C5	B	305	34.63#	21.17	105	21	18	82.19	45	3831.42
	C6	N	305	34.55#	21.8	116.5	23.3	19	86.76	45	-
	C7	B	225	29.3	17.13	95	19	1	4.57	45	-
	C8	B	150	21.88	15.17	88	17.6	0.0083	0.038	45	2918.13
	C9	N	305	34.55#	21.4	109.5	21.9	18	82.19	0	-

578

579 $\gamma' \approx 7$ kN/m^3 (kaolin clay) and 4.5 kN/m^3 (calcareous silt)

580 # Applied spring tension

581 * Accounting for non-uniform acceleration field (radius for 200 g was set at 1/3 of soil sample

582 depth)

583 + Excluding time required for ramp down, anchor setting at 1 g and ramp back again to 200 g

584 **Table 2.** Model and prototype anchor dimensions

Dimension	Symbol	Anchor B		Anchor N	
		Model*	Prototype	Model*	Prototype
Anchor length	L_A	75 mm	15 m	81.5 mm	16.3 m
Anchor diameter	D_A	6 mm	1.2 m	6 mm	1.2 m
Tip length	L_T	11.2 mm	2.24 m	10.5 mm	2.1 m
Fin[+] length	L_F	50 mm	10 m	37 mm	7.4 m
Fin width	w_F	4.5 mm	0.9 m	10.75 mm[#]	2.15 m
Fin thickness	t_F	0.5 mm	0.1 m	0.5 mm	0.1 m
Dry weight	W_{dry}	19.16 gm	1504 kN	22.01 gm	1727 kN

585

586 [+] Number of fin = 4

587 * The models are made from brass (density = 8400 kg/m^3)

588 [#] Maximum width

589

590 **Table 3.** Engineering properties of kaolin clay (data from Stewart, 1992)

Property	Value
Liquid limit, LL (%)	61
Plastic limit, PL (%)	27
Plasticity index, I_p (%)	34
Specific gravity, G_s	2.6
Consolidation coefficient (mean), c_v (m^2/year)	~2.6
Sensitivity, S_t	2.5~3

591

592 **Table 4.** Engineering properties of calcareous silt

Property	Value
Liquid limit, LL (%)	76
Plastic limit, PL (%)	35
Plasticity index, I_p (%)	41
Specific gravity, G_s	2.77
Consolidation coefficient (mean), c_v (m^2/year)	~12
Sensitivity, S_t	5

593

594

595 **Figure Captions**

596 **Fig. 1.** Typical torpedo anchors with 4 fins (after de Aguiar et al. 2009)

597 **Fig. 2.** Torpedo anchor installation procedure

598 **Fig. 3.** Data from field tests carried out at the Campos Basin, offshore Brazil and Gjøa field,
599 North Sea (Medeiros 2002; de Araujo et al. 2004; Brandão et al. 2006; Lieng et al. 2010): (a)
600 Effect of seabed soil type and stratigraphy on anchor penetration depth; (b) Measured anchor
601 penetration depth in clay for different drop height and impact velocity; (c) Theoretical
602 prediction of impact velocity for various C_d; (d) Effect of load inclination and consolidation
603 time (t_c) on holding capacity

604 **Fig. 4.** Model anchors used in centrifuge tests (1:200)

605 **Fig. 5.** Anchor release system in drum centrifuge: (a) before releasing anchor; (b) after
606 releasing and installing anchor

607 **Fig. 6.** Anchor pullout at various angles in drum centrifuge (kaolin clay): (a) 80°; (b) 45°; (c)
608 0°

609 **Fig. 7.** Anchor pullout at various angles in drum centrifuge (calcareous silt): (a) 80°; (b) 45°;
610 (c) 0°

611 **Fig. 8.** Preparation of clay and silt sample together dividing drum channel into two
612 compartments: (a) View of full channel divided into two compartments; (b) After
613 consolidation; (c) After scraping

614 **Fig. 9.** Shear strength profiles from T-bar tests ($N_{T\text{-}bar}$ = 10.5)

615 **Fig. 10.** Impact velocities from centrifuge tests and reported data: (a) Typical dynamic
616 installation profile of a torpedo anchor (Test C7, Table 1); (b) Achieved impact velocities and
617 theoretical prediction (accounting for non-uniform acceleration field); (c) Comparison
618 between results from this study and reported data from model and field tests

619 **Fig. 11.** Embedment depths from centrifuge tests and reported data

620 **Fig. 12.** Top view at the mudline after installing the anchor: (a) Kaolin clay; (b) Calcareous
621 silt

622 **Fig. 13.** Effect of soil type on pullout resistance ($\theta_0 = 45°$, Tests K7, K9 and C5, C8; Table 1)

623 **Fig. 14.** Effect of pullout angle, θ_0, on pullout resistance (model B, K2, K4, K7 and C3~C5;
624 Table 1): (a) Kaolin clay; (b) Calcareous silt

625 **Fig. 15.** Effect of time allowed for reconsolidation, t_c, on pullout resistance: (a) $\theta_0 = 0°$
626 (models B and N, Tests K3, K10 and C1, C4; Table 1); (b) $\theta_0 = 45°$ (model B, Tests K7~K9,
627 and C5, C8; Table 1)

628 **Fig. 16.** Effect of non-dimensional time, T, on normalised holding capacity

629 **Fig. 17.** Effect of model anchor geometry on pullout resistance (clay): (a) $\theta_0 = 0°$ (Tests K2,
630 K3; Table 1); (b) $\theta_0 = 45°$ (Tests K6, K7; Table 1)

631

632

633

634

635 

636 (a) Torpedo anchors (After de Aguiar et al. 2009)

637 

638 (b) Torpedo anchors (after Salies 2004)

639 **Figure 1. Typical torpedo anchors with 4 fins**

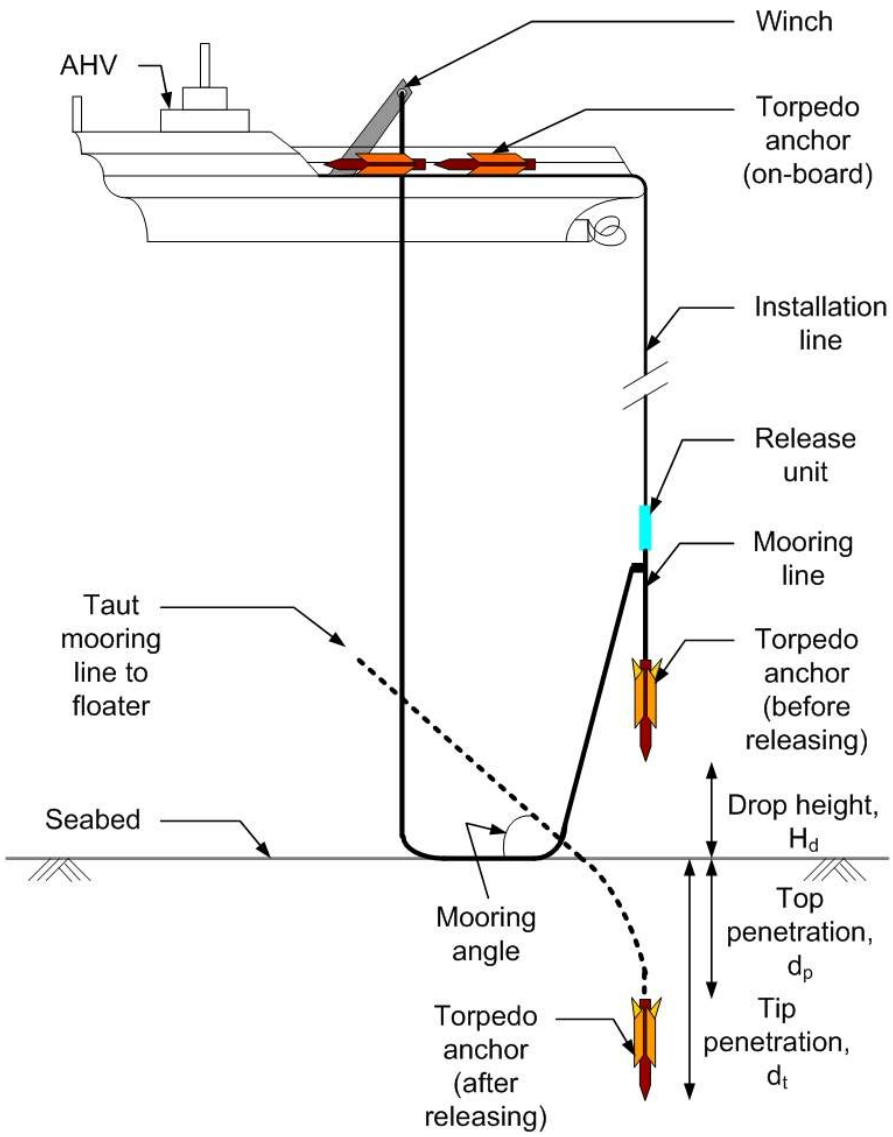

640

641 **Figure 2. Torpedo anchor installation procedure**

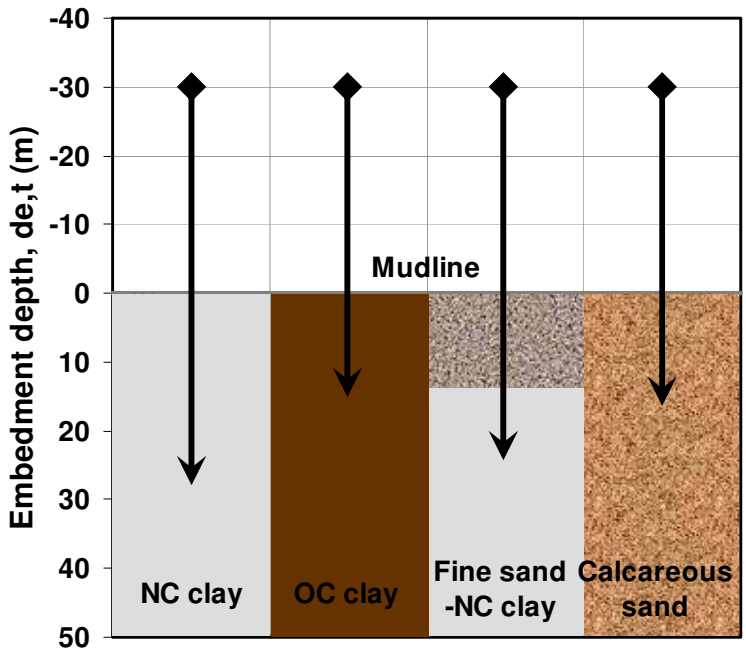

642

643 (a) Effect of seabed soil type and stratigraphy on anchor penetration depth

644

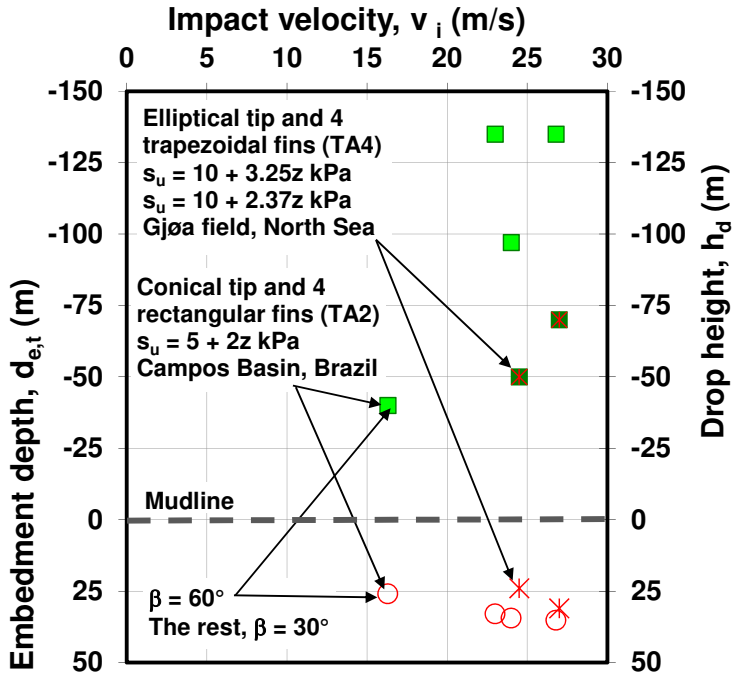

645

646 (b) Measured anchor penetration depth in clay for different drop height and impact velocity

647

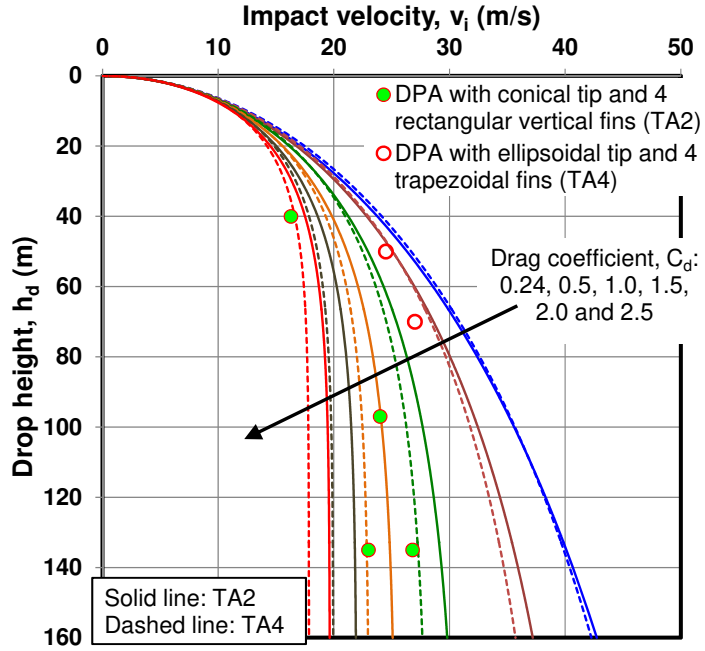

(c) Theoretical prediction of impact velocity for various C_d

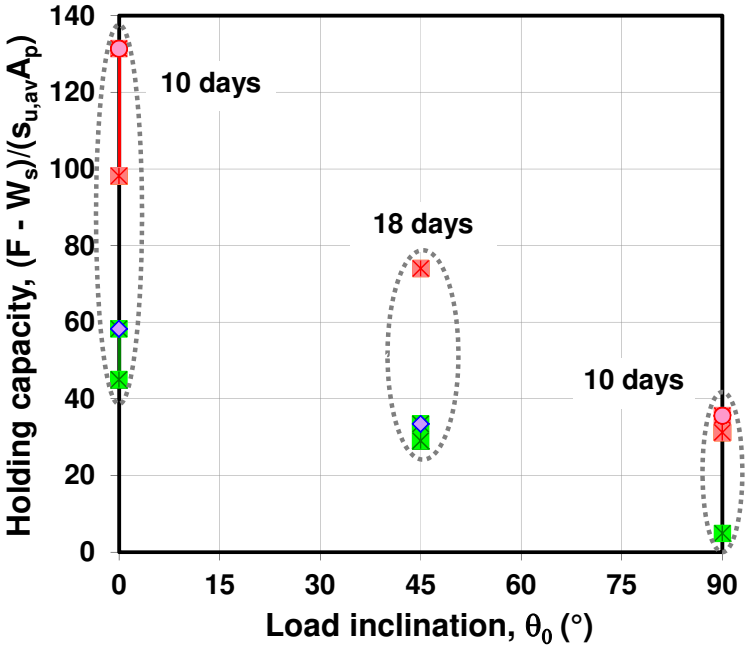

(d) Effect of load inclination and consolidation time (t_c) on holding capacity

Figure 3. Data from field tests carried out at the Campos Basin, offshore Brazil and Gjøa field, North Sea (Medeiros 2002; de Araujo et al. 2004; Brandão et al. 2006; Lieng et al. 2010)

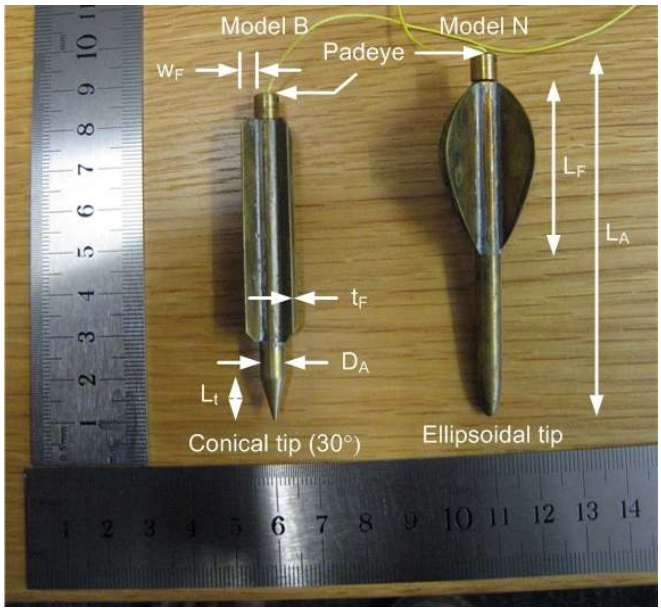

Figure 4. Model anchors used in centrifuge tests (1:200)

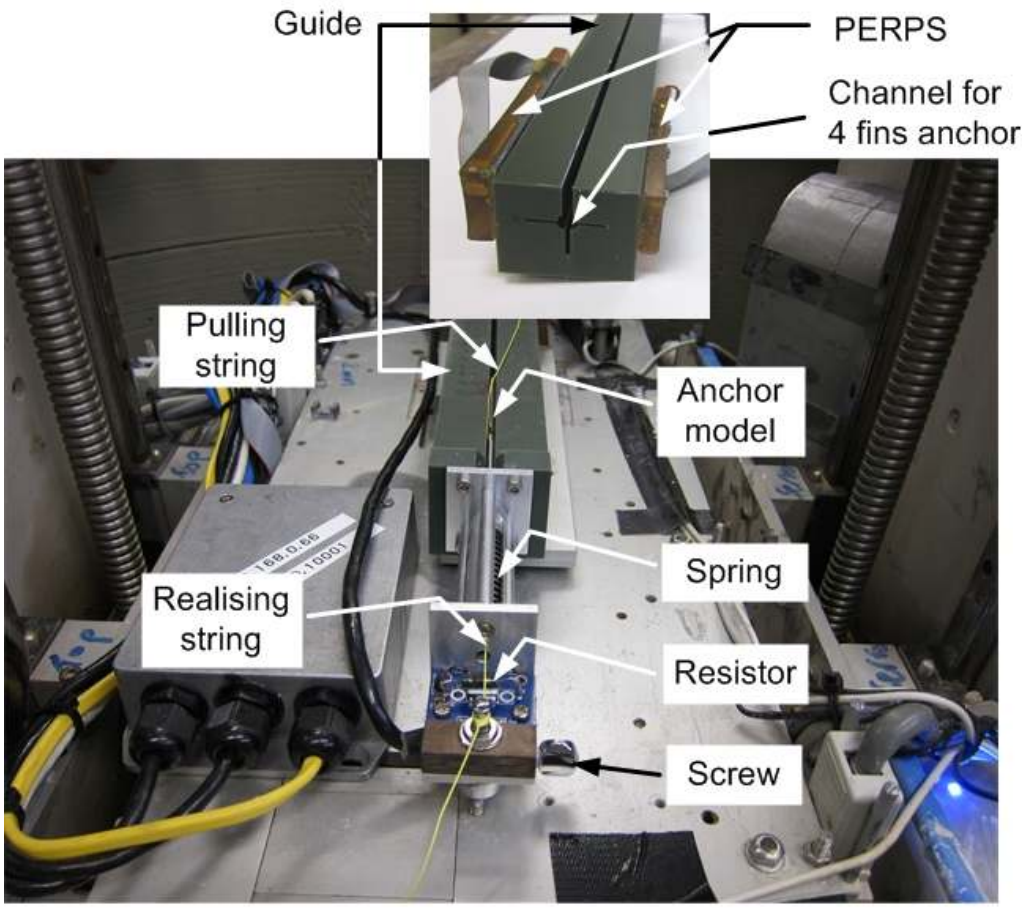

(a) Before releasing anchor

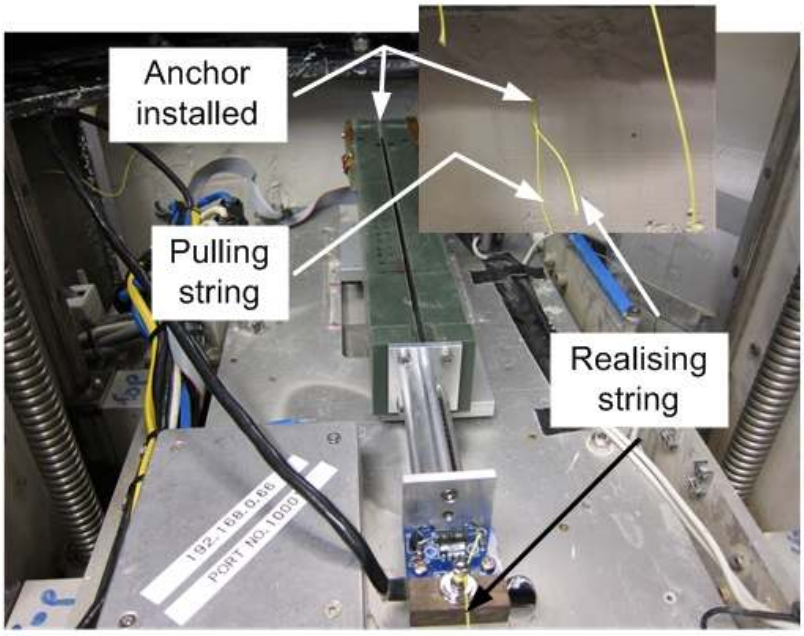

(b) After releasing and installing anchor

Figure 5. Anchor release system in drum centrifuge

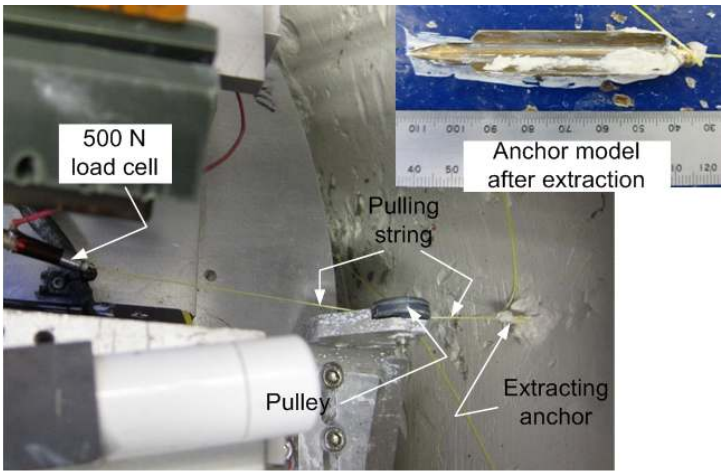

(a) 80° pull-out

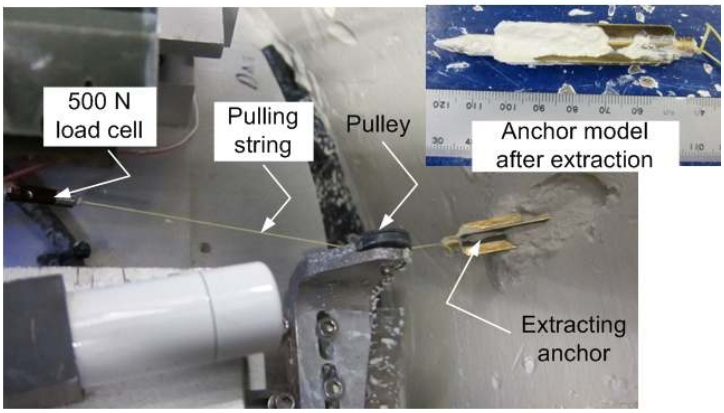

(b) 45° pull-out

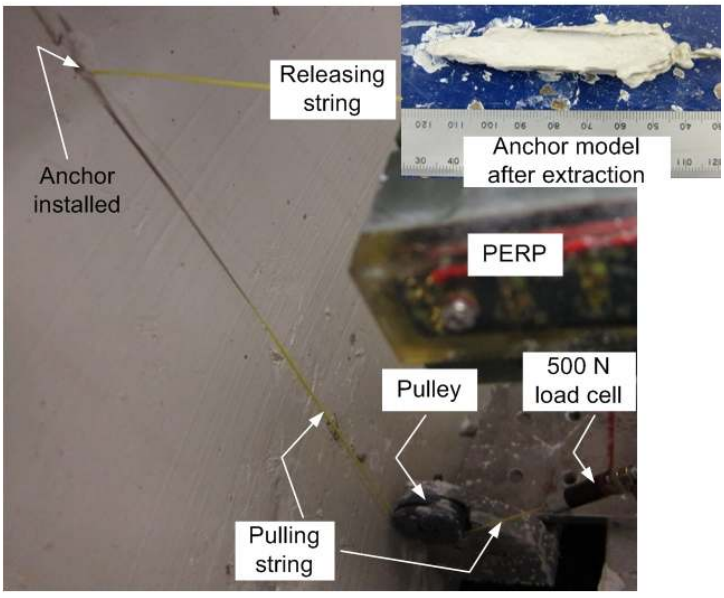

660 (c) 0° pull-out

661 **Figure 6. Anchor pullout at various angles in drum centrifuge (kaolin clay)**

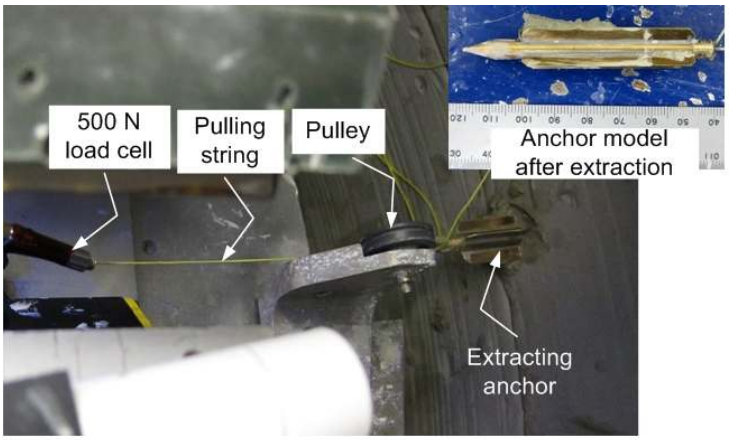

(a) 80° pull-out

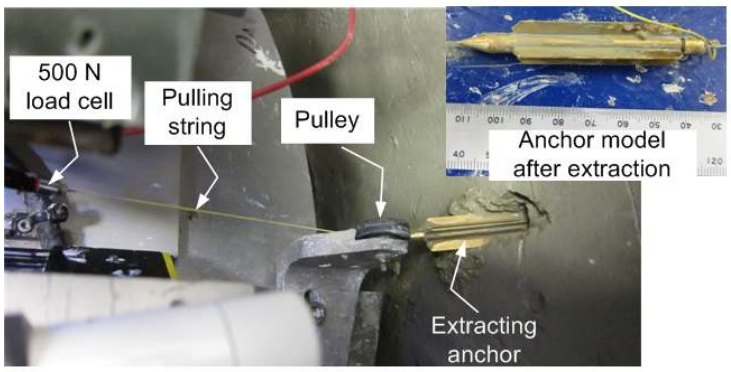

(b) 45° pull-out

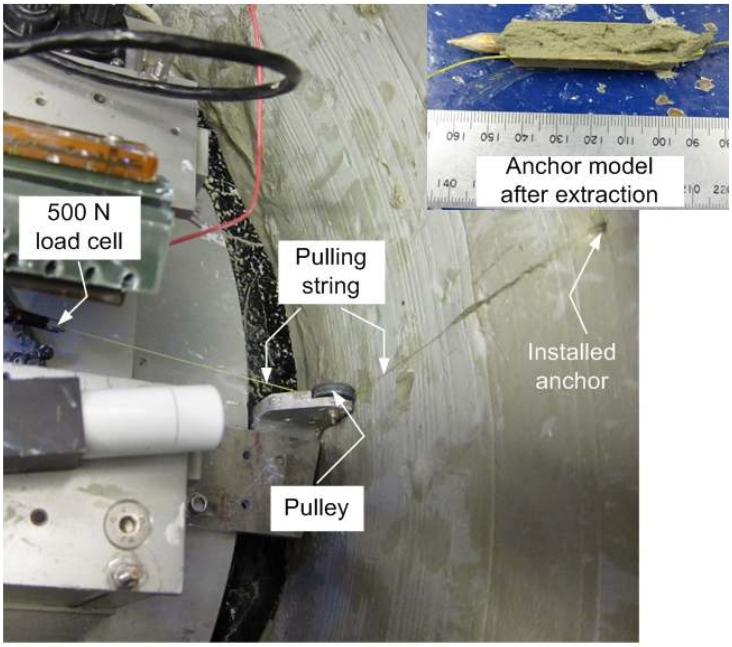

(c) 0° pull-out

Figure 7. Anchor pullout at various angles in drum centrifuge (calcareous silt)

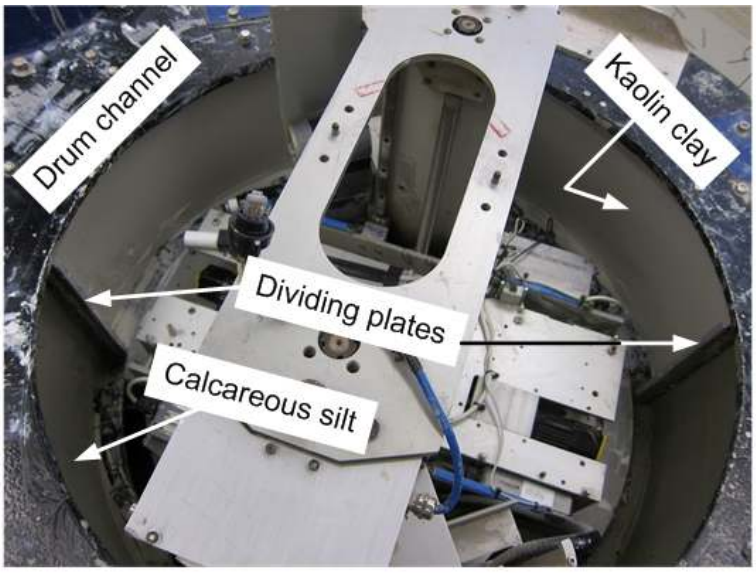

(a) View of full channel divided into two compartments

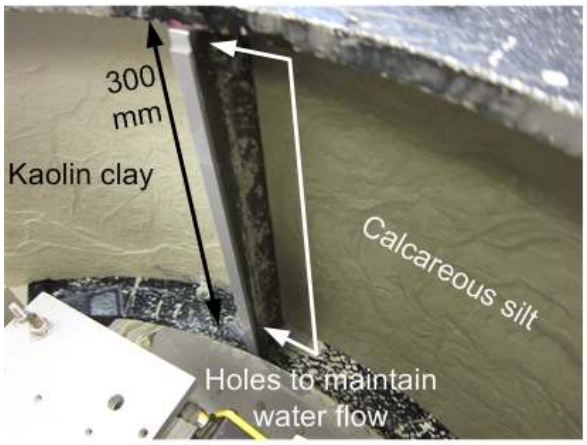

(b) After consolidation

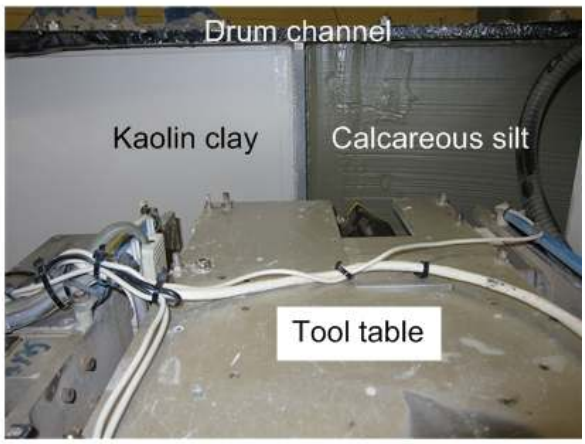

(c) After scrapping

665

666 **Figure 8. Preparation of clay and silt sample together dividing drum channel into two**
667 **compartments**

668

669

670

671

672

673

674

675

676

677

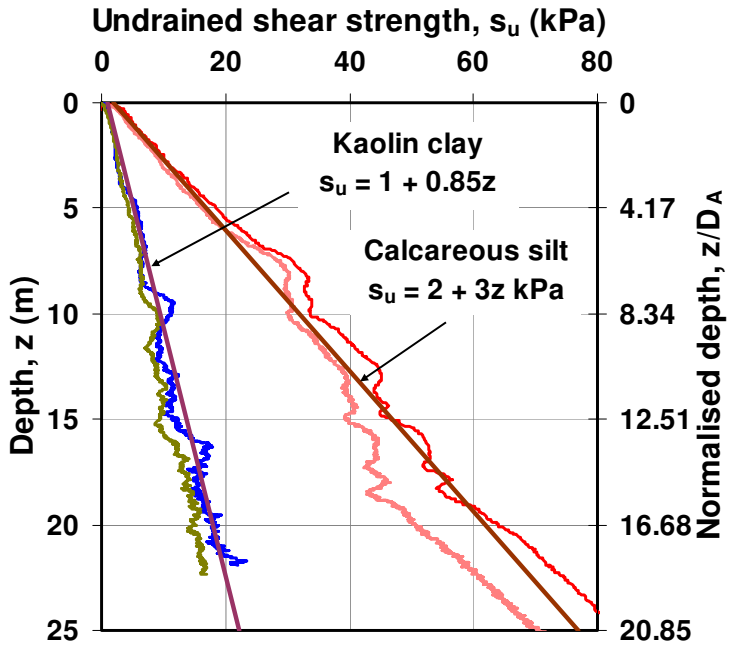

678

679 **Figure 9. Shear strength profiles from T-bar tests ($N_{T\text{-}bar}$ = 10.5)**

680

681

682

683

684

685

686

687

688

689

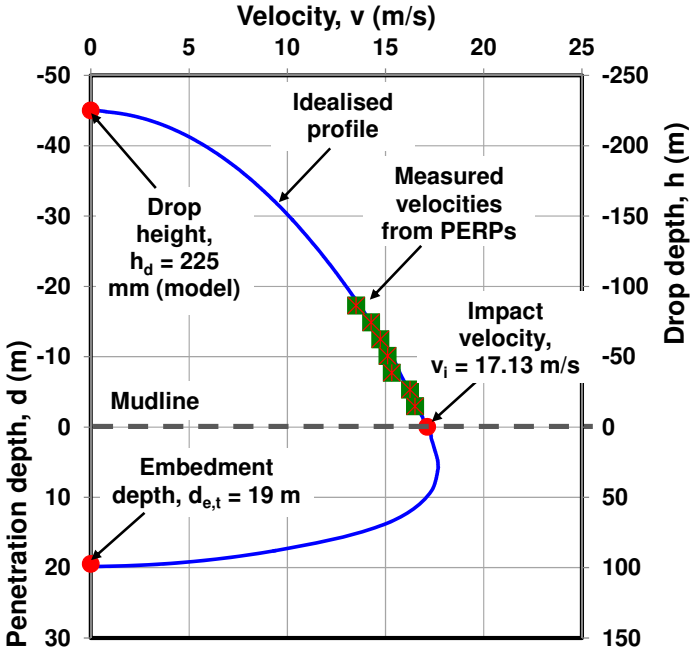

690

691 (a) Typical installation profile of a DPA (Test C7, Table 1)

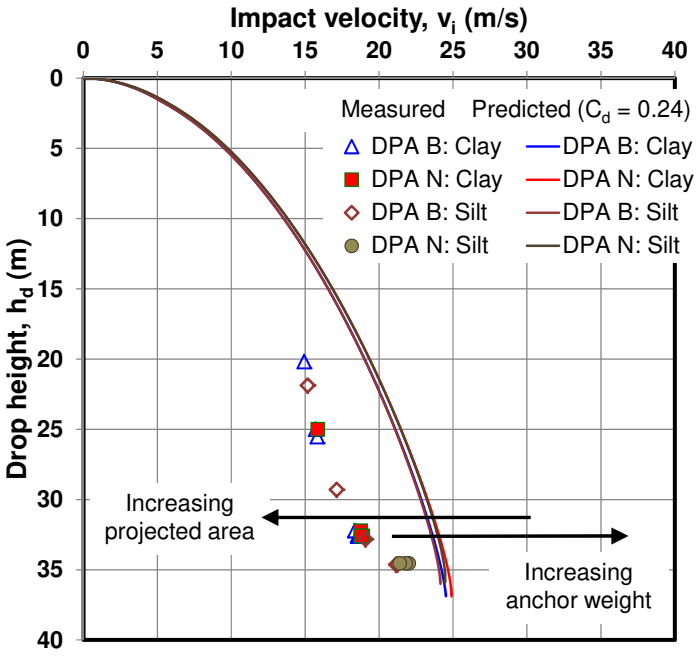

692

693 (b) Achieved impact velocities and theoretical prediction (accounting for non-uniform

694 acceleration field)

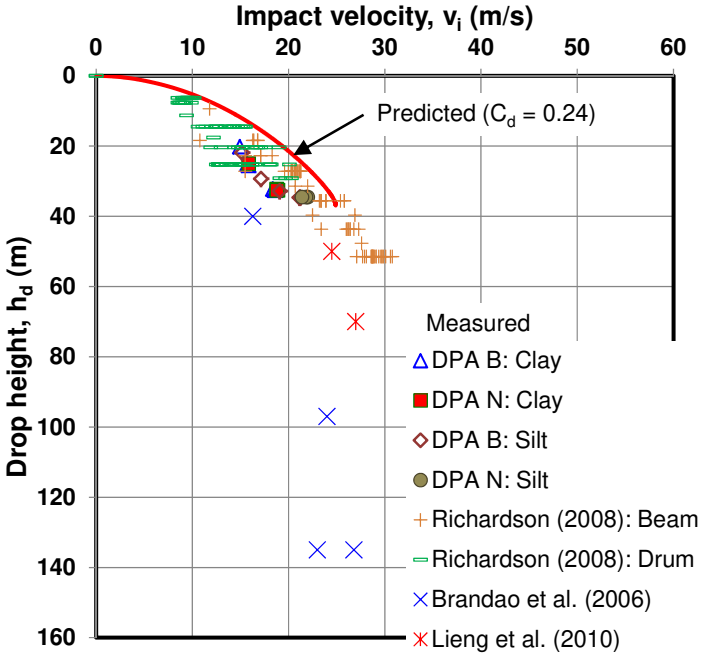

(c) Comparison between results from this study and reported data from model and field tests

Figure 10. Impact velocities from centrifuge tests and reported data

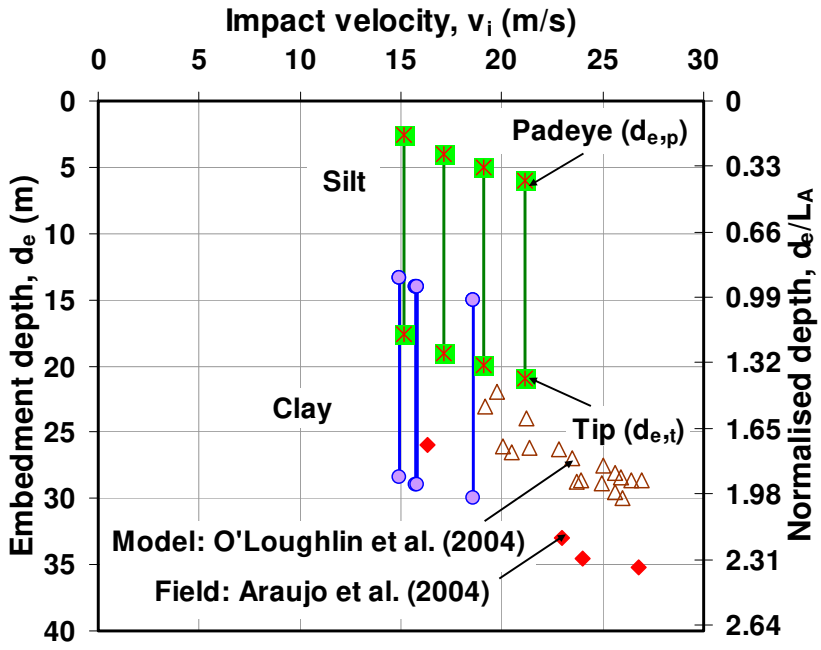

701

702 **Figure 11. Embedment depths from centrifuge tests and reported data**

(a) Kaolin clay (b) Calcareous silt

703

704 **Figure 12. Top view at the mudline after installing the anchor**

705

706

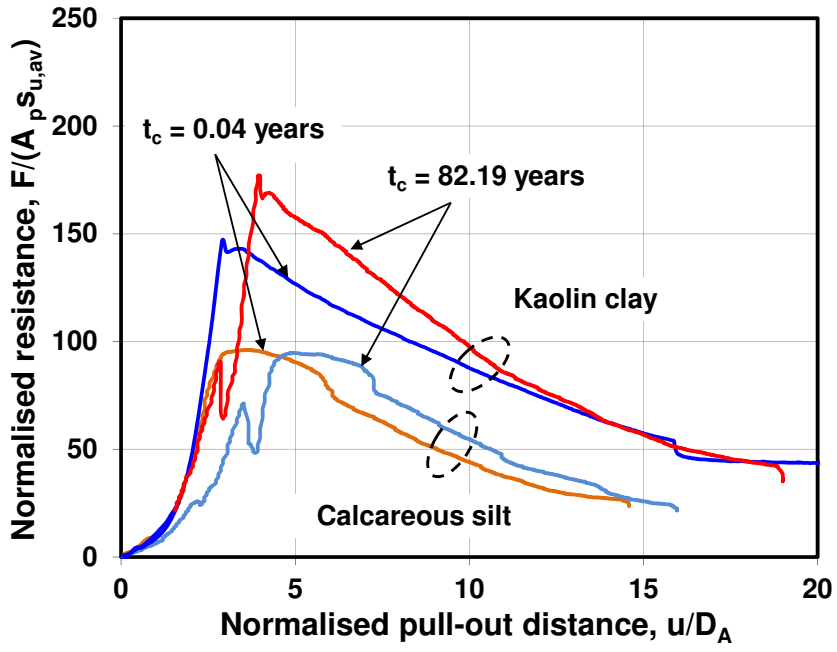

707

708 **Figure 13. Effect of soil type on pullout resistance (θ_0 = 45°, Tests K7, K9 and C5, C8;**
709 **Table 1)**

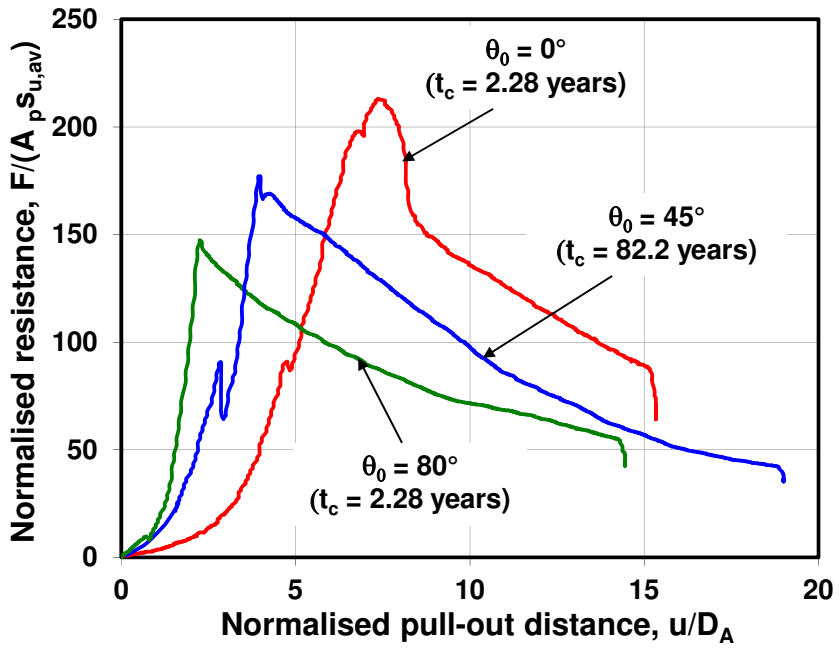

710

711 (a) Kaolin clay

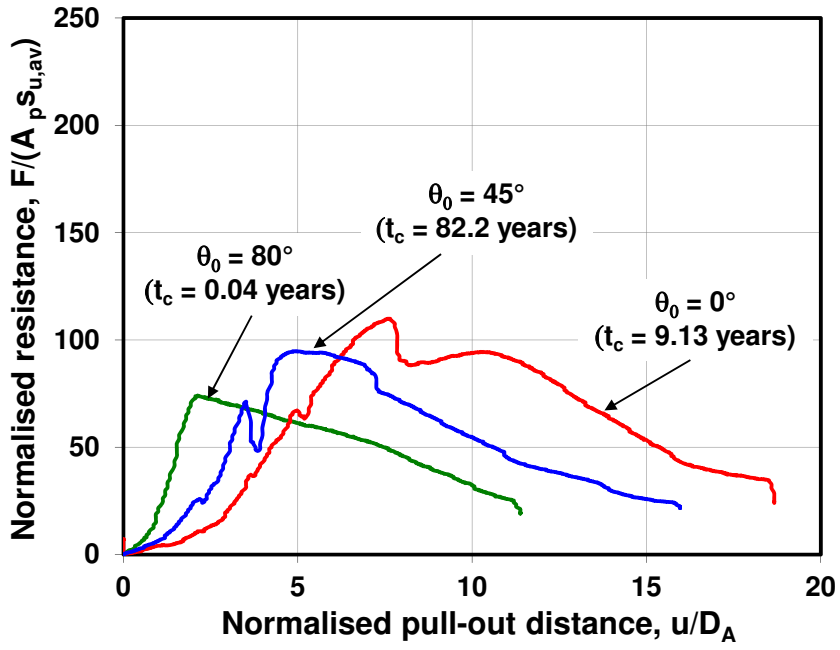

712

713 (b) Calcareous silt

714 **Figure 14. Effect of pullout angle, θ_0, on pullout resistance (model B, K2, K4, K7 and**
715 **C3~C5; Table 1)**

716

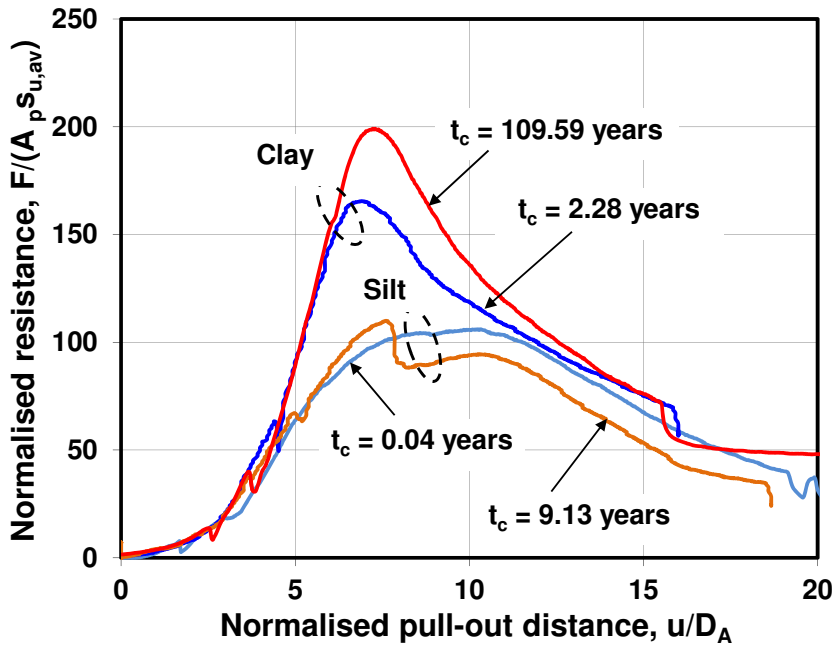

717

718 (a) $\theta_0 = 0°$ (models B and N, Tests K3, K10 and C1, C4; Table 1)

719

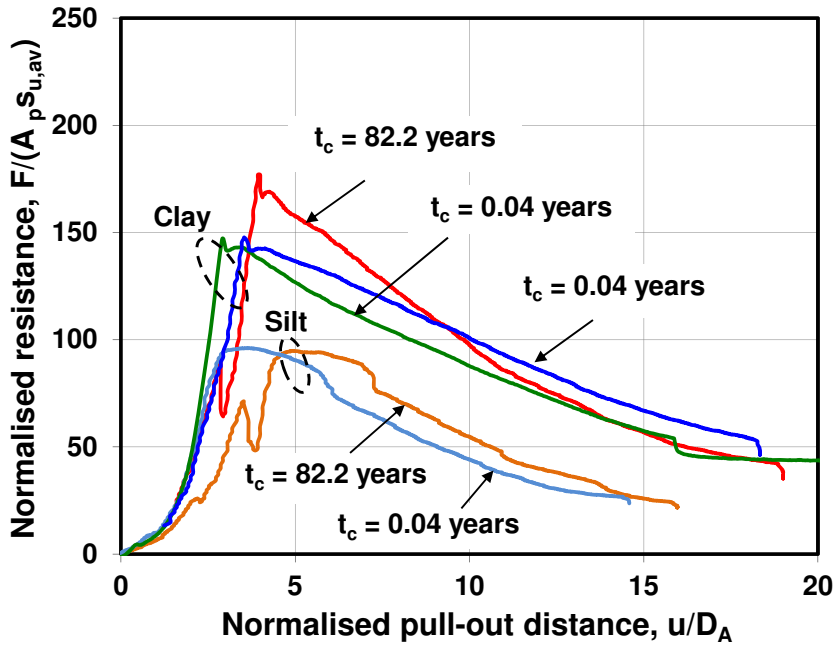

720

721 (b) $\theta_0 = 45°$ (model B, Tests K7~K9, and C5, C8; Table 1)

722 **Figure 15. Effect of time allowed for reconsolidation, t_c, on pullout resistance**

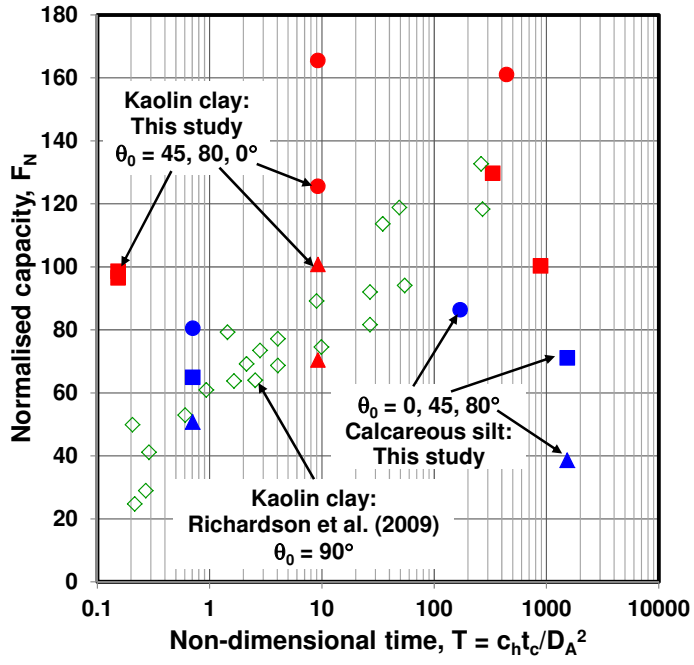

723

724 **Figure 16. Effect of non-dimensional time, T, on normalised holding capacity**

725

726

727

728

729

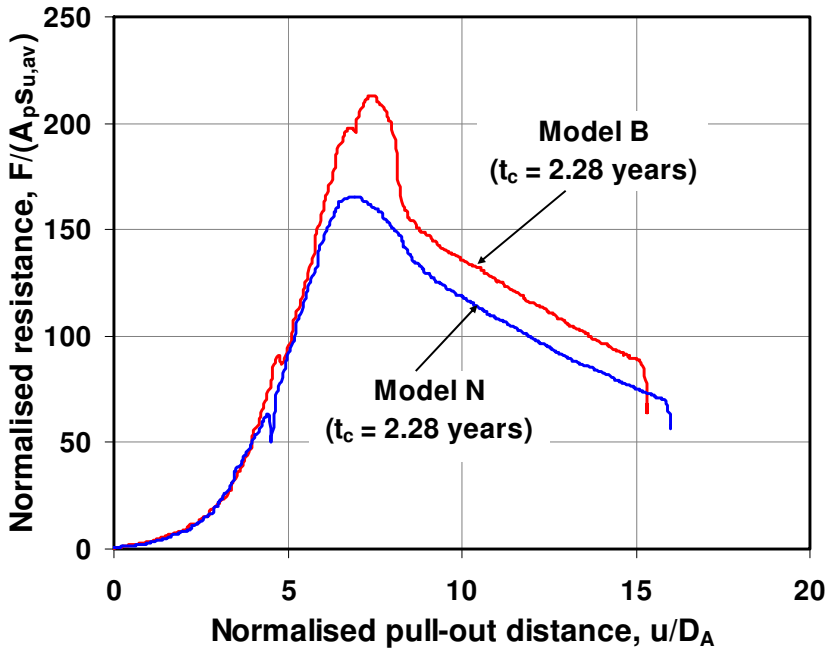

730

731 (a) $\theta_0 = 0°$ (Tests K2, K3; Table 1)

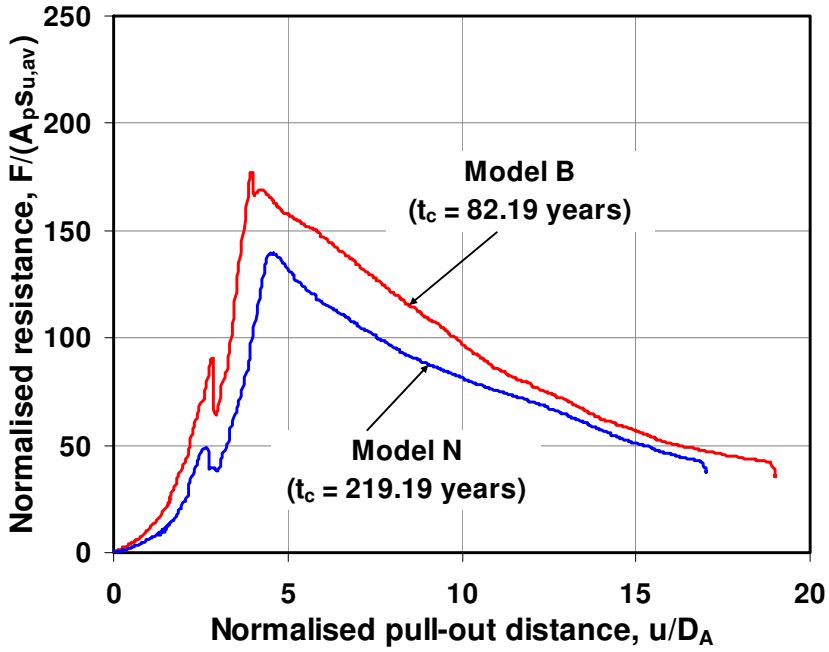

732

733 (b) $\theta_0 = 45°$ (Tests K6, K7; Table 1)

734 **Figure 17. Effect of model anchor geometry on pullout resistance (clay)**

735

736